# CFD SIMULATION APPLICATION TO EVALUATE AND ENHANCE THE HOMOGENITY OF AIR DISTRIBUTION IN HEAT PUMP DRYER

## ỨNG DỤNG MÔ PHỎNG CFD ĐỂ ĐÁNH GIÁ VÀ NÂNG CAO ĐỘ ĐỒNG ĐỀU CỦA PHÂN BỐ TÁC NHÂN SẤY TRONG THIẾT BỊ SẤY BƠM NHIỆT

**Nguyen Duc Trung[1,*], Nguyen Truong Giang[1], Nguyen Duc Nam[2], An Dai Duc[1], Nguyen Duc Huy[1], Pham Duc Binh[1], Nguyen Huu Khai[1], Nguyen Thi Thao[3]**

DOI: http://doi.org/10.57001/huih5804.2024.217

**ABSTRACT**

One of the most critical processes in the food industry is drying, but most drying equipment suffers from non-uniform air distribution. Applying the CFD simulation to tune the configuration or change the tray install method of drying equipment improves drying efficiency. This study shows the effect of different numbers of trays (case 25, 18, 13 trays) and the improved configuration (13 trays with varying tray angles) on the air distribution of the drying chamber. The most appropriate case is the new configuration, which has more air uniformity by installing two air shields near the inlet and outlet and changing the angle of the trays.

***Keywords:*** *CFD, drying process, uniform drying, tray dryer, COMSOL multiphysics.*

**TÓM TẮT**

Một trong những quá trình quan trọng nhất trong ngành công nghiệp thực phẩm là quá trình sấy, nhưng hầu hết các thiết bị sấy đều không có phân bố không khí đồng đều. Ứng dụng mô phỏng CFD để tinh chỉnh thiết bị sấy giúp cải thiện hiệu suất sấy. Bài nghiên cứu này cho thấy ảnh hưởng của các cấu hình khay (trường hợp 25, 18, 13 khay) và cấu hình cải tiến (13 khay với các góc nghiêng khay khác nhau) đến phân bố gió trong thiết bị. Trường hợp phù hợp nhất là trường hợp ứng dụng phương pháp xếp khay mới, có phân bố không khí đều hơn trong thiết bị nhờ lắp đặt thêm hai tấm chắn gió ngay gần cửa gió vào và cửa gió ra và thay đổi góc nghiêng của khay.

***Từ khóa:*** *CFD, quá trình sấy, sấy đồng đều, thiết bị sấy dạng khay, COMSOL multiphysics.*

[1]School of Chemistry and Life Sciences, Hanoi University of Science and Technology, Vietnam
[2]Faculty of Electrical Engineering, Hanoi University of Industry, Vietnam
[3]LIFEFOOD CO.,LTD, Vietnam
[*]Email: trung.nguyenduc@hust.edu.vn
Received: 28/11/2023
Revised: 15/3/2024
Accepted: 25/6/2024

### 1. INTRODUCTION

The main objective of drying food is to remove moisture and prevent the growth of bacteria, yeast, and mold that can spoil it [1]. After the drying process, a good part of the vitamins, minerals, and flavors of food are preserved [2]. Several drawbacks exist, such as low drying efficiency, product moisture inhomogeneity, and high energy consumption due to uneven air distribution in the convection drying equipment [3]. The CFD simulation conducted by Dazza-Gómez et al. indicates that due to poor air distribution in the drying chamber, trays 2, 3, and 4 receive a significant amount of air, while the others receive less [4], so it can lead to inhomogeneity of moisture content of the products.

Previously, the method to improve drying equipment was building and testing pilot-scale models multiple times, which took a lot of time and cost. Nowadays, with technological advancements, the food industry has extensively implemented Computational Fluid Dynamics (CFD) to surmount these issues [5]. CFD method uses techniques from physics, math, and computer science to model and predict fluid and liquid flow motion [6].

CFD is used to predict the air velocity profiles as well as air uniformity in the equipment with the most appropriate k-ε model [7]. Several studies using CFD simulations experimented with tuning the shape and angle of the air vane guide at the inlet of the equipment [8], adding the wind deflector [9] and the guide air cover [10]. All of the above achieve the configuration with fairly even air distribution, which proves the effectiveness of the CFD simulation.

### 2. MATERIALS AND METHODS

#### 2.1. Governing equations

The Navier-Stokes equation describes the fluid motion, but obtaining analytical solutions is difficult. Numerical

methods, especially CFD, are widely used to solve the equation, even for complex problems [11]. In turbulent flow mode, all quantities fluctuate in time and space; the Reynolds-averaged Navier-Stokes (RANS) equations are used:

$$\rho\frac{\partial U}{\partial t}+\rho(U\cdot\nabla)U+\nabla\cdot\overline{(\rho u'\otimes u')} = \nabla\cdot\mu(\nabla U+(\nabla U)^{T})+F-\nabla P \quad (1)$$

$$\rho\nabla\cdot U=0 \quad (2)$$

$$\nabla.\overline{(\rho u'\otimes u')} \quad (3)$$

The notation U represents the average velocity field and $\otimes$ denotes the outer vector product. The term $\nabla\cdot U$ represents the divergence of the average velocity field. Equation (3) refers to the Reynolds stress tensor, which captures the interaction between the fluctuating components of the velocity field. The k-ε model adds two transport equations and two dependent variables (turbulent kinetic energy k and turbulent dissipation rate ε) to further analyze turbulent flows [12]:

$$\rho\frac{\partial k}{\partial t}+\rho u\cdot\nabla k=\nabla\cdot\left(\left(\mu+\frac{\mu_T}{\sigma_k}\right)\nabla k\right)+P_k-\rho\varepsilon \quad (4)$$

$$P_k=\mu_T\left(\nabla u:\left(\nabla u+(\nabla u)^{T}\right)-\frac{2}{3}(\nabla.u)^2\right)-\frac{2}{3}\rho k\nabla.u \quad (5)$$

$$\rho\frac{\partial\varepsilon}{\partial t}+\rho u.\nabla\varepsilon=\nabla.\left(\left(\mu+\frac{\mu_T}{\sigma_\varepsilon}\right)\nabla\varepsilon\right)+C_{\varepsilon1}\frac{\varepsilon}{k}P_k-C_{\varepsilon2}\rho\frac{\varepsilon^2}{k} \quad (6)$$

Equation (4) is the transport equation for k, equation (6) is for ε, and equation (5) represents the production term. Constants $C_\mu$, $C_{\varepsilon1}$, $C_{\varepsilon2}$, $\sigma_k$, and $\sigma_\varepsilon$ are assigned specific values such as $C_\mu = 0.09$, $C_{\varepsilon1} = 1.44$, $C_{\varepsilon2} = 1.92$, $\sigma_k = 1$, and $\sigma_\varepsilon = 1.3$.

### 2.2. Equipment modeling

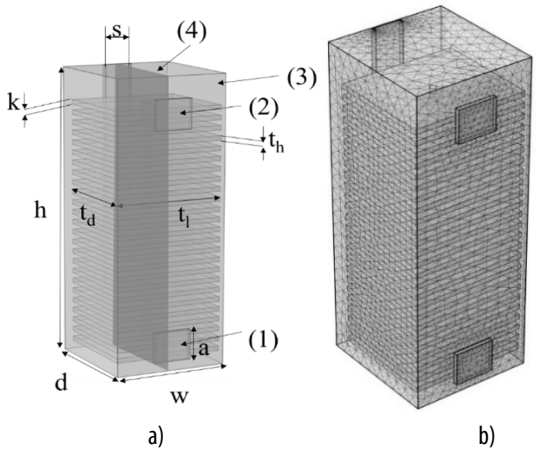


Fig. 1. Equipment descriptions and simulation meshing

The three-dimensional models are simulated in COMSOL Multiphysics 6.0®. The dimensions of the inlet and outlet are equal. The simulation model only represents the drying chamber, trays, and the inlet and outlet. Other components of the equipment are omitted from the model to reduce its complexity without affecting the simulation result. Fig. 1 shows the dimensions of the equipment. The surface (4) is the symmetry plane of the model.

Table 1. Equipment dimensions and main details

| Symbol | Description | Value (mm) | Symbol | Description | Value (mm) |
|---|---|---|---|---|---|
| a | Inlet/Outlet width | 198 | k | Trays spacing | 55 |
| b | Inlet/Outlet height | 164 | h | Chamber height | 1586 |
| $t_l$ | Tray length | 578 | w | Chamber width | 600 |
| $t_h$ | Tray height | 25 | d | Chamber depth | 630 |
| $t_d$ | Tray depth | 520 | s | Wind conduct | 140 |
| - | Top air shield length | 600 | - | Bottom air shield length | 600 |
| - | Top air shield width | 658 | - | Bottom air shield width | 600 |
| - | Top air shield height | 5 | - | Bottom air shield height | 5 |

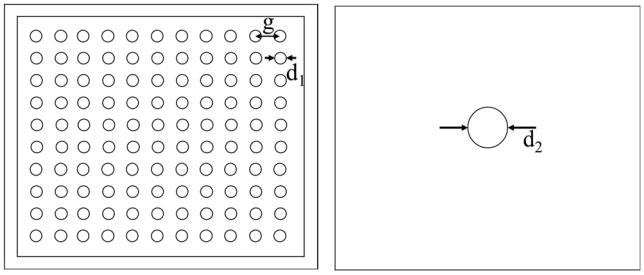


Fig. 2. Perforated trays in the drying process and model trays used in the simulation

The simulation model assumed that the material fill the trays during the drying process. The block in the model represents the perforated trays with drying material. Perforated trays are simplified to the tray with one big hole in the middle to reduce the complexity of the simulation model. The small holes are 5mm ($d_2$) in diameter, with a spacing (g) of 5mm. The air leak through all the small holes is equivalent to the amount of air through the big hole that is 20mm in diameter after calculating.

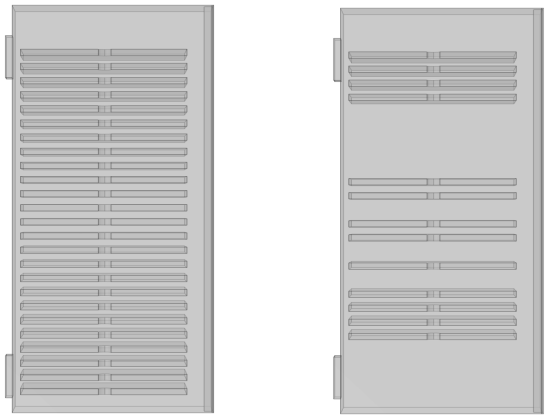

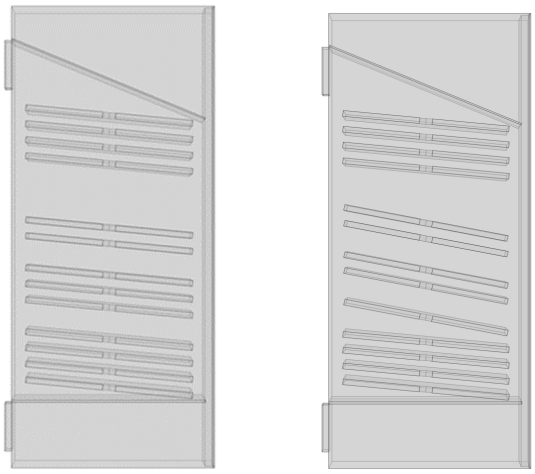

c) First improved configuration d) Second improved configuration

Fig. 3. View at the cut plane (4) of five configurations

The first improved configuration changed all the tray's angles to six degrees. The second improved configuration increases the angle of 5th to 9th trays to 12 degrees. The two air shields are installed on the top and the bottom of the chamber, with the air shield at the top having a 24-degree angle.

### 2.3. Meshing and boundary conditions

Table 2 shows the mesh element size and boundary conditions set for the simulation. All the simulation cases use the same boundary conditions and meshing in the boundary following Table 2.

Table 2. Boundary conditions and meshing

| Boundaries | Value/ Type | Mesh element size | Largest/smallest size of a mesh (mm) |
|---|---|---|---|
| Inlet (1) | v = 14m/s | Fine | 0.159/0.0285 |
| Outlet (2) | p = $10^5$Pa | Fine | 0.159/0.0285 |
| Wall (3) | Slip condition | Coarse | 0.301/0.0634 |
| Symmetry (4) | - | Coarse | 0.301/0.0634 |

As the drying chamber is symmetrical, only half of the model is simulated to save time without affecting the total results. The model is meshed with tetrahedral cells. The inlet and outlet mesh are fine mesh element sizes, while the others only need coarse element sizes.

### 2.4. Evaluation criterion

This study uses the following criterion to evaluate the amount of air going through the material surface and the air distribution in the equipment.

$$v_{avg} = \frac{\sum v_i}{n} \quad (7)$$

$$\sigma_v = \sqrt{\frac{\sum (v_i - v_{avg})^2}{n}} \quad (8)$$

$$\sigma_{\%} = \frac{\sigma_v}{v_{avg}} \times 100(\%) \quad (9)$$

$$\delta = \frac{v_{max} - v_{min}}{v_{avg}} \quad (10)$$

Table 3. Notations definition

| Notation | Description | Definition |
|---|---|---|
| $v_i$ | The effective velocity of the material surface on $i^{th}$ tray | The average velocity value of finite points on the evaluated surfaces. |
| $v_{avg}$ | The pretension velocity | Evaluate the amount of air going through the material surface. |
| n | Number of trays | - |
| $\sigma_v$ | The standard deviation of the $v_i$ value of the case | Measure the amount of variation or dispersion of the $v_i$ set. |
| $\sigma_{\%}$ | Coefficient of velocity variation | The coefficient to evaluate the correlation between the velocity dispersion and the pretension velocity achieved. |
| $\delta$ | The coefficient of the actual difference velocity. | The relative variability of the $v_i$ set. |

## 3. RESULTS AND DISCUSSION

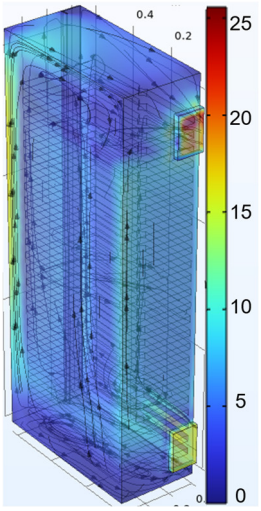


a) 25 trays

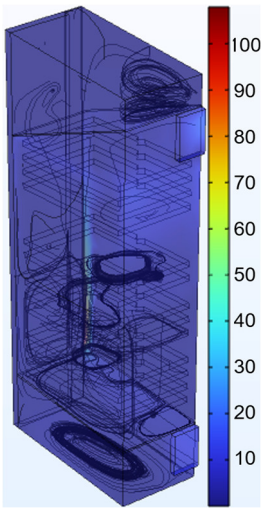


b) First improved configuration

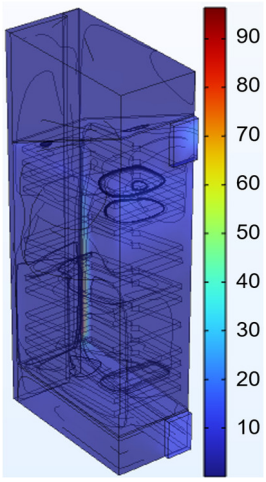


c) Second improved configuration

Fig. 4. Velocity contour of equipment with different configurations

In a 25-tray configuration, dry air enters the inlet and through the last four trays. The relative humidity of the air increases and tends to move directly into the air duct. The moist air ascends and a part of it through the upper trays, while only a small quantity of air moves through the middle of the chamber (from 7$^{th}$ to 19$^{th}$ trays) and goes to the outlet. The trays are arranged very closely (only 55mm apart) with a high outlet, which causes the air to blow directly from the inlet into the wind conduct and up to the outlet.

Table 4. The average air velocity on the surface of each tray (25-tray configuration)

| N° | $v_i$ (m/s) | N° | $v_i$ (m/s) | N° | $v_i$ (m/s) | N° | $v_i$ (m/s) | N° | $v_i$ (m/s) |
|---|---|---|---|---|---|---|---|---|---|
| 1 | 0.640 | 6 | 0.104 | 11 | 0.035 | 16 | 0.077 | 21 | 0.302 |
| 2 | 1.165 | 7 | 0.051 | 12 | 0.036 | 17 | 0.070 | 22 | 0.464 |
| 3 | 1.088 | 8 | 0.025 | 13 | 0.049 | 18 | 0.069 | 23 | 1.841 |
| 4 | 0.483 | 9 | 0.027 | 14 | 0.064 | 19 | 0.095 | 24 | 2.846 |
| 5 | 0.203 | 10 | 0.030 | 15 | 0.069 | 20 | 0.178 | 25 | 2.898 |

The first four trays, especially trays 2 and 3, receive a lot of air. Because of the small amount of air passing through, the materials on the trays in the middle section have low mass transfer dynamics and have higher moisture content than the trays in the top and bottom sections after the drying process.

Table 5. The average air velocity on each tray of the last three cases

| 13 trays | | 1$^{st}$ improved configuration | | 2$^{nd}$ improved configuration | |
|---|---|---|---|---|---|
| N° | $v_i$ (m/s) | N° | $v_i$ (m/s) | N° | $v_i$ (m/s) |
| 1 | 0.461 | 1 | 1.244 | 1 | 1.222 |
| 2 | 1.155 | 2 | 0.785 | 2 | 0.765 |
| 3 | 1.175 | 3 | 0.403 | 3 | 0.451 |
| 4 | 0.429 | 4 | 0.289 | 4 | 0.407 |
| 5 | 0.121 | 5 | 0.349 | 5 | 0.498 |
| 6 | 0.237 | 6 | 0.299 | 6 | 0.468 |
| 7 | 0.133 | 7 | 0.350 | 7 | 0.422 |
| 8 | 0.105 | 8 | 0.386 | 8 | 0.371 |
| 9 | 0.120 | 9 | 0.412 | 9 | 0.347 |
| 10 | 0.226 | 10 | 0.315 | 10 | 0.336 |
| 11 | 0.731 | 11 | 0.377 | 11 | 0.351 |
| 12 | 2.143 | 12 | 0.403 | 12 | 0.391 |
| 13 | 2.330 | 13 | 0.510 | 13 | 0.404 |

Table 6. Evaluated criterion calculated for the last three configurations

| Config. / Criterion | 25 trays | 13 trays | 1$^{st}$ improved configuration | 2$^{nd}$ improved configuration |
|---|---|---|---|---|
| $v_{ag}$ | 0.516 | **0.720** | 0.471 | 0.495 |
| $\sigma_{\%}$ | 162% | 107% | 56% | **50%** |
| $\delta$ | 55.639 | 3.088 | 2.029 | **1.791** |

In Case 2, all trays near the inlet are uninstalled to avoid problems with the first configurations. This configuration has a low $v_i$ value from 5$^{th}$ to 10$^{th}$ trays. On the remaining trays, the material tends to have low moisture loss, and the product may not meet the moisture content desired after the drying process.

Through observing the velocity contour of previous configurations, the air tends to go towards the outlet, so case 3 adds two air shields to direct the air in from the inlet and directly through the wind conduct, then go up and divide into multiple streamlines passing through trays. The trays are also tilted at a 6-degree angle to increase the air-receiving area, and the air unformity is better than the previous configurations, as shown by the decrease in two criterion. In the final case, by increasing the angle of five trays in the middle to 12 degrees, their air-receiving area is increased, and this case has the most even air distribution, making it the appropriate configuration for the drying equipment to reach the product moisture homogeneity.

## 4. CONCLUSION

The uniformity of air distribution in the drying equipment is a factor affecting the uniformity of product moisture content**.** CFD simulation is an effective tool for predicting air distribution of several configurations tested. This study shows that in this evaluated drying equipment with fewer trays near the inlet and middle of the chamber, the uniform of air distribution is improved. The trays must be tilted to have more air through the tray surface. Also, those in the middle must have higher angles than the others. The last configuration is appropriate, in which each four trays near the inlet and outlet, five trays in the middle, and two air shields at the top and bottom of the drying equipment are correspondingly inclined at 6 degrees, 12 degrees, and 24 degrees.

**REFERENCES**

[1]. Patel KK., Kar A., "Heat pump assisted drying of agricultural produce - An overview," *J Food Sci Technol*, 49, 142-160, 2012.

[2]. Loemba ABT., Kichonge B., Selemani JR., Kivevele T., "Performance evaluation of solar-assisted "lokheat pump dryer integrated with thermal energy storage for drying Moringa Oleifera leaves," *MRS Adv*, 8, 698-702, 2023.

[3]. Bie Y., Li M., Guo XY., Sun JG., Qiu Y., "Experimental study on improving the drying uniformity in hot air cross-flow dryer," *IOP Conf Ser Earth Environ Sci*, 93, 2017.

[4]. Daza-Gómez MAM., Gómez Velasco CA., Gómez Daza JC., Ratkovich N., "3D Computational Fluid Dynamics Analysis of a Convective Drying Chamber," Processes, 10, 2721, 2022.

[5]. Darabi H., Zomorodian A., Akbari MH., Lorestani AN., "Configuration a cabinet dryer with two geometric configurations using CFD," *J Food Sci Technol*, 52, 359-366, 2013.

[6]. Thabet S., Thabit TH., "Computational Fluid Dynamics: Science of the Future," *International Journal of Research and Engineering*, 5, 430-433, 2018.

[7]. Misha S., Mat S., Ruslan M.H., Sopian K., E. Salleh, "The Prediction of Drying Uniformity in Tray Dryer System using CFD Simulation," *International Journal of Machine Learning and Computing,* 3(5): 419-423, 2013.

[8]. Chen HH., Huang TC., Tsai CH., Mujumdar A., "Development and performance analysis of a new solar energy-assisted photocatalytic dryer," *Drying Technology*, 26, 503-507, 2008.

[9]. Shi M., Zhang Y., Wang Y., Gao M., Li J., Deng Z., Liu R., Li M., "Flow field analysis and configuration optimisation of Tibetan medicine double heat pump drying room," *Comput Electron Agric,* 199, 107141, 2022.

[10]. Hui-hui S., Ping Y., Le-Yang F., Xin-yue Z., "Numerical Simulation of Hot Air Drying Kiln Velocity Field Based on Computational Fluid Dynamics," *International Journal of Research in Engineering and Science* (IJRES), 3, 5, 09-13, 2015.

[11]. Sheng W., "A revisit of Navier-Stokes equation," *European Journal of Mechanics - B/Fluids*, 80, 60-71, 2020.

[12]. CFD Module User's Guide. 178–184. Accessed 17 September 2023. <URL: https://doc.comsol.com/5.4/doc/com.comsol.help.cfd/CFDModuleUsersGuide.pdf>

[13]. Akdemir S., Arin S., "Spatial Variability of Ambient Temperature, Relative Humidity and Air Velocity in a Cold Store," *J Cent Eur Agric*, 7, 101-110, 2006.

**THÔNG TIN TÁC GIẢ**

**Nguyễn Đức Trung[1], Nguyễn Trường Giang[1], Nguyễn Đức Nam[2], An Đại Đức[1], Nguyễn Đức Huy[1], Phạm Đức Bình[1], Nguyễn Hữu Khải[1], Nguyễn Thị Thảo[3].**

[1]Trường Hóa và Khoa học sự sống, Đại học Bách khoa Hà Nội

[2]Khoa Điện, Trường Đại học Công nghiệp Hà Nội

[3]Công ty TNHH Thực phẩm Cuộc sống